

Article

Influence of Sample Preparation on SERS Signal

Isabela Bianchi-Carvalho ¹, Marcelo José dos Santos Oliveira ¹, Cibely Silva Martin ²,
Santiago Sánchez-Cortés ³ and Carlos José Leopoldo Constantino ^{1,*}

¹ School of Technology and Sciences, São Paulo State University (UNESP),
Presidente Prudente 19060-900, SP, Brazil; isabela.bianchi-carvalho@unesp.br (I.B.-C.);
marcelo.oliveira@unesp.br (M.J.d.S.O.)

² School of Engineering, São Paulo State University (UNESP), Ilha Solteira 15385-007, SP, Brazil;
cibely.martin@unesp.br

³ Instituto de Estructura de la Materia, Instituto de Estructura de la Materia-Consejo Superior de
Investigaciones Científicas (IEM-CSIC), 28006 Madrid, Spain; s.sanchez.cortes@csic.es

* Correspondence: carlos.constantino@unesp.br

Abstract: Carbendazim (MBC), a commonly used fungicide from the benzimidazole group, was applied in this study as a probe molecule to understand the influence of sample preparation on the SERS (surface-enhanced Raman scattering) signal. We applied the external standard method (ESM), preparing fresh Ag colloid samples (reduced by hydroxylamine) for each concentration and measuring with and without potassium nitrate (KNO₃) as an aggregation-inducing salt. The impact of sample dilution before or after the addition of the salt to the Ag colloid was also explored. SERS signals were correlated with Ag colloid aggregation observed via transmission electron microscopy (TEM), UV-Vis extinction, dynamic light scattering (DLS), and zeta potential, examining diffusion-limited cluster aggregation (DLCA) and reaction-limited cluster aggregation (RLCA) mechanisms. The optimal results were achieved without KNO₃, with more compact aggregates at lower concentrations and more branched ones at higher concentrations. Dilution of the Ag colloid before salt addition enabled lower detection limits than without any dilution. No SERS signal was observed when the salt was added before dilution. These findings emphasize that a consistent relationship between aggregate morphology and the SERS signal cannot be generalized across analytes. Analyte-specific properties play a crucial role in determining optimal aggregation conditions for SERS analysis.



Received: 31 October 2024

Revised: 8 January 2025

Accepted: 16 January 2025

Published: 18 January 2025

Citation: Bianchi-Carvalho, I.;
Oliveira, M.J.d.S.; Martin, C.S.;
Sánchez-Cortés, S.; Constantino, C.J.L.
Influence of Sample Preparation on
SERS Signal. *Chemosensors* **2025**, *13*, 22.
[https://doi.org/10.3390/
chemosensors13010022](https://doi.org/10.3390/chemosensors13010022)

Copyright: © 2025 by the authors.
Licensee MDPI, Basel, Switzerland.
This article is an open access article
distributed under the terms and
conditions of the Creative Commons
Attribution (CC BY) license
([https://creativecommons.org/
licenses/by/4.0/](https://creativecommons.org/licenses/by/4.0/)).

Keywords: aggregation mechanism; carbendazim; SERS; detection

1. Introduction

Carbendazim (MBC) is a widely used fungicide belonging to the benzimidazole group. Its mechanism of action involves inhibiting β -tubulin polymerization, thereby disrupting the formation of the mitotic spindle and hindering cell division [1]. In agriculture, it can be applied to crops such as cotton, sugarcane, rice, beans, and soy for leaf and seed treatment [1]. Its use was banned in Brazil in 2022 and in Europe in 2016 due to its potential carcinogenic effects on humans and concerns regarding reproductive toxicity and mutagenicity [2].

MBC detection using surface-enhanced Raman spectroscopy (SERS) has been demonstrated in a large list of published works. SERS became a prominent technique due to its exceptional sensitivity and selectivity. However, this technique presents challenges in its analytical application, since fluctuations in the intensity of the SERS signal are frequent, given that the amplification factor is related to the dielectric functions (in the wavelength of

the incident laser) of the metallic nanostructures and the medium where they are embedded (usually air or water); the morphology (shape and dimension) and spatial distribution (level of aggregation) of the metallic nanostructures; and the mechanism of adsorption of the target molecule on the metallic nanostructures (direct adsorption favors amplification).

Most of the works found in the literature use sophisticated experimental procedures. In Ref. [3], a dual-function Au@MIP (gold nanoparticle surface molecularly imprinted polymers) was employed to evaluate MBC traces by SERS, resonance Rayleigh scattering (RRS), and absorption analysis. In Ref. [4], the multiple detection of MBC and imidacloprid was performed based on color- and Raman-encoded SERS-LFA (lateral flow immunoassay). Real samples (cucumber, apple, and lake water) were also analyzed. In Ref. [5], a 3D SERS substrate was utilized, where ZnO nanorods (ZnO NRs) decorated with multi-shaped silver nanoparticles (MAg NPs) were fabricated on polydimethylsiloxane (PDMS). Some other works use Au substrates for MBC detection. In Ref. [6], a Au colloid prepared by the reduction of chloroauric acid with sodium citrate was used to determine the MBC concentration in tea leaves. In Ref. [7], spherical and monodispersed Au colloids were synthesized using the sodium citrate reduction method for MBC detection in Tieguanyin oolong tea.

Previously in our research group, Furini et al. [8] used Ag colloids reduced with hydroxylamine and sodium citrate and Au colloids reduced with sodium citrate for MBC detection, varying the excitation laser in the SERS technique as well as the MBC concentration. As a result, they obtained the best detection conditions with the Ag colloid, which was reduced by hydroxylamine at a pH of 6, and found out that the adsorption of MBC particles on a AgNP surface occurs via the nitrogen atom of the imidazole group. In Ref. [9], they conducted a study on the influence of pH variation on MBC detection via SERS using a Ag colloid reduced with hydroxylamine along with DFT calculations. It was observed that neutral MBC binds to the metal via the nitrogen atom of the imidazole ring, while deprotonated MBC can attach through the imidazole nitrogen in conjunction with either the nitrogen atom of the amide group or the oxygen atom of the carbonyl group.

In this work, we aim to study how sample preparation influences the SERS signal using MBC as a probe molecule, considering all the available data found in the literature on MBC. The ESM method was applied for the measurements, in which a new sample is prepared using an aliquot of a neat Ag colloid for each MBC concentration. For better comprehension, a comparison can be made with the SAM (standard addition method), in which the MBC aliquots are added consecutively to the same aliquot of Ag colloid. A Ag colloid reduced by hydroxylamine was used, and measurements were conducted both in the presence and absence of salt (potassium nitrate). In the latter case, we examined conditions with and without the dilution of the Ag colloid prior to MBC addition and varied the order of dilution. The role of the aggregated Ag colloid on the SERS signal was investigated through a combination of transmission electron microscopy (TEM) images, UV-Vis extinction spectroscopy, size distribution measurements by dynamic light scattering (DLS), and zeta potential, and by considering the different aggregation mechanisms that can occur (DLCA: diffusion-limited cluster aggregation or RLCA: reaction-limited cluster aggregation).

2. Materials and Methods

2.1. Reagents

Hydroxylamine hydrochloride ($\text{NH}_2\text{OH}\cdot\text{HCl}$), sodium hydroxide (NaOH), and silver nitrate (AgNO_3) from Sigma-Aldrich (St. Louis, MO, USA) were used in the Ag colloid synthesis. MBC (Sigma-Aldrich, St. Louis, MO, USA; 99% purity) was applied as the analyte for SERS detection. KNO_3 was acquired from Sigma-Aldrich (St. Louis, MO, USA;

Analytical grade). The Ag colloid was prepared in ultrapure water from a Milli-Q system (Direct-Q 3UV, Merck KGaA, Darmstadt, GER; 18.2 M Ω .cm—pH 5.6). MBC solutions were prepared in ultrapure water and ethanol.

2.2. Ag Colloid Synthesis

The colloid with silver nanoparticles (AgNPs) was synthesized using the method employed by Oliveira and collaborators [10], originally described by Leopold and Lendl [11]. In simple terms, the procedure involves the addition of 300 μ L of sodium hydroxide (1.0 mol/L) to 90 mL of an aqueous solution of hydroxylamine hydrochloride (1.66×10^{-3} mol/L), under constant magnetic stirring. After 5 min, 10 mL of an aqueous solution of silver nitrate (AgNO_3 1.0 $\times 10^{-2}$ mol/L) was added drop by drop. The resulting dispersion was kept under agitation for 15 min, and it is necessary to wait at least 24 h before it can be used in experiments.

2.3. MBC Stock Solution Preparation

Initially, a stock solution of MBC at 1.0×10^{-3} mol/L in ethanol was prepared. Other stock solutions of MBC were prepared by diluting the latter solution in water. In this way, solutions at 1.0×10^{-4} mol/L, 1.0×10^{-5} mol/L, and 1.0×10^{-6} mol/L were obtained.

2.4. MBC in Ag Colloid Sample Preparation

2.4.1. In the Absence of Potassium Nitrate

- UV-Vis extinction, DLS, and zeta potential: 2000 μ L of ultrapure water and 500 μ L of the Ag colloid were mixed. Then, 10 samples of MBC were prepared as shown in Table S1 and Figure S1.
- SERS: 2500 μ L of the Ag colloid to prepare MBC samples according to Table S1 and Figure S1.
- TEM: The colloidal dispersion was dried on a grid following the same conditions of SERS measurements for the Ag colloid in the absence of MBC and in the presence of MBC with final concentrations of 1.0×10^{-6} mol/L, 1.6×10^{-6} mol/L, 4.0×10^{-6} mol/L, 9.7×10^{-6} mol/L, and 2.4×10^{-5} mol/L.

2.4.2. In the Presence of Potassium Nitrate: Without Ag Colloid Dilution

- SERS: 100 μ L of a 0.5 mol/L solution of potassium nitrate (KNO_3) was added to 2500 μ L of the Ag colloid. Then, 100 μ L of the total volume of the colloidal dispersion was removed and MBC was added following Table S1.

2.4.3. In the Presence of Potassium Nitrate: With Ag Colloid Dilution

- UV-Vis extinction, DLS, zeta potential, and SERS: 2000 μ L of ultrapure water, 500 μ L of Ag colloid, and 100 μ L of 0.5 mol/L solution of KNO_3 were mixed following two different orders:
 1. Dilution before aggregation: ultrapure water was added to the Ag colloid before the addition of salt.
 2. Aggregation before dilution: salt was added to the Ag colloid before ultrapure water.

Then, 100 μ L of the total volume of the colloidal dispersion (Ag colloid + water + salt for both orders) was removed and MBC was added. The additions were performed initially with the least concentrated stock solution (1.0×10^{-6} mol/L) up to the most concentrated (1.0×10^{-3} mol/L—in ethanol), as shown in Table S1 and Figure S1.

2.5. Measurement Acquisition

2.5.1. UV-Vis Extinction

- In the absence of potassium nitrate—The measurements were performed in a spectrophotometer UV-Vis-NIR Shimadzu 3600 (Shimadzu, Kyoto, JAP) equipped with a photomultiplier tube (PMT—photomultiplier tube) for the UV-Vis region, and InGaAs and PbS detectors for near-infrared (NIR—near infrared).
- In the presence of potassium nitrate: with Ag colloid dilution—Varian spectrophotometer, model Cary 50 (Varian, Palo Alto, CA, USA), utilizing quartz cuvettes with a 10 mm optical path.

2.5.2. Raman and SERS

- In the absence of potassium nitrate—Portable spectrometer Raman Virsa (Renishaw, Wotton-under-Edge, UK) with a 785 nm laser. A 50× objective long focal lens and an integration time of 10 s were employed.
- In the presence of potassium nitrate: with and without Ag colloid dilution—Renishaw in-Via micro-Raman spectrograph (Renishaw, Wotton-under-Edge, ENG) equipped with a CCD detector and a 1200 l/mm diffraction grating for the 785 nm laser. An exposure time of 10 s and 10% power were used for the 50× objective long focal lens (Leica Germany, Wetzlar, GER; numerical aperture 0.5—model 566036).
- The spectra were collected from a sample droplet, with the laser beam focused on the liquid-air interface. The laser power measured for the 785 nm laser line was 330 mW, and 80 mW after the 50× lens (in-Via) and 50 mW (Virsa).

2.5.3. DLS and Zeta Potential:

- In the absence of potassium nitrate and in the presence of potassium nitrate: with Ag colloid dilution—Zetasizer Nano ZS90 (Malvern).

2.5.4. TEM Images:

- In the absence of potassium nitrate, they were obtained at the Universidad Complutense de Madrid (Madrid, ES), using JEM 1400 Plus (JEOL, Tokyo, JAP) equipment with acceleration voltage from 40 to 120 kV at intervals of 33 V. The TEM mode presents a resolution of 0.38 nm between points and 0.2 nm between lines, with magnification ranging from 50× to 12,105×. The camera has a focal length of 15 to 350 cm in AS DIFF and from 4 to 80 cm in HD DIFF, and the electron cannon is of the thermionic type with a LaB6 filament.

3. Results

3.1. In the Absence of Potassium Nitrate

3.1.1. SERS

Analyzing the measurements conducted in the absence of salt, the first SERS signal was obtained at 1.0×10^{-6} mol/L with an intensity of 3164 ± 519 counts (Figure 1a). The limit of detection (LOD) was calculated based on the definition by Richard L. McCreery in the book “Raman Spectroscopy for Chemical Analysis” [12] using the band at 1288 cm^{-1} as a reference. According to the author, a Raman signal is detectable when the SERS signal intensity is at least three times greater than the intensity of the noise in the Ag colloid spectrum in the absence of MBC [12]. Thus, in our case, a LOD of 2.0×10^{-7} mol/L was observed. The SERS signal increases linearly between MBC concentrations of 1.0×10^{-6} mol/L and 3.0×10^{-6} mol/L (Figure 1b,c). Before this optimal concentration, it is possible that not all surfaces of the Ag nanoparticles (AgNPs) were covered with MBC, causing residual charges and electrostatic repulsion that limited aggregation. However, at 3.0×10^{-6} mol/L, the

entire surface of the AgNPs might be covered, optimizing aggregation and the SERS signal. Above 3.0×10^{-6} mol/L, the SERS signal reaches a saturation plateau, which is consistent with the entire covered surface of the AgNPs, leading to an excess of MBC molecules in the colloid. Therefore, since the surface of the AgNPs is already completely covered, the addition of more MBC does not contribute to an increase in the SERS signal anymore [13].

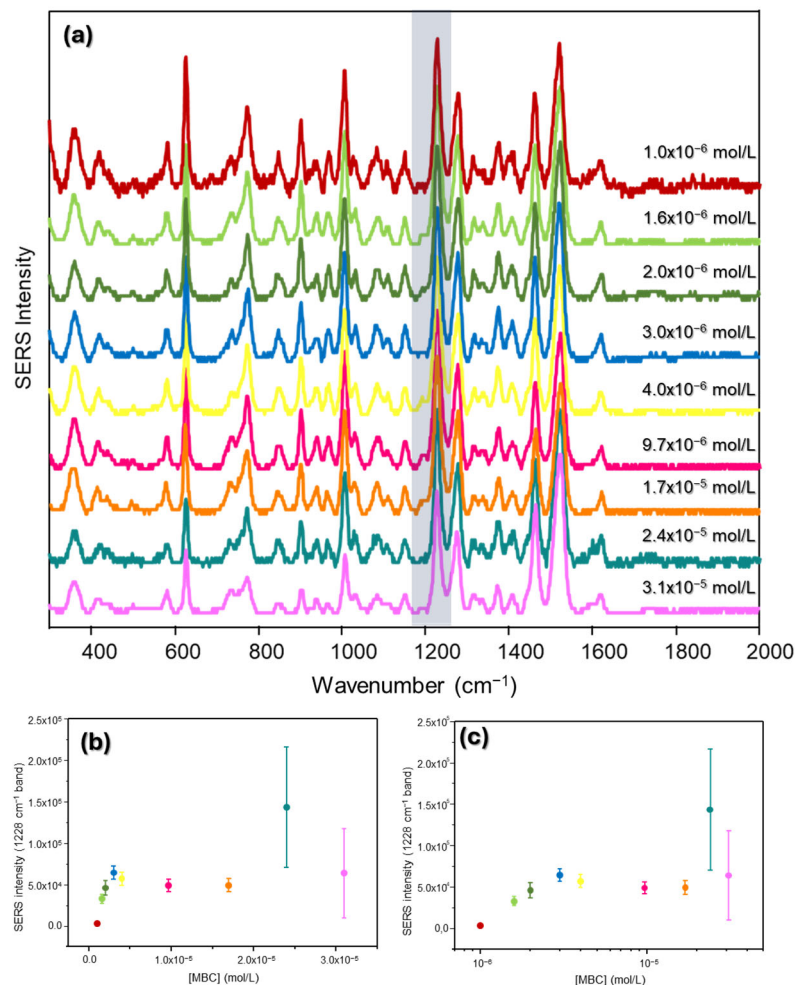


Figure 1. (a) SERS spectra of MBC in a Ag colloid (not diluted) in the absence of salt. Laser at 785 nm, 1 accumulation, acquisition time of 10 s. The laser power varied for each concentration; however, all intensities were calculated based on the maximum power (65 mW). Spectra with baseline correction and normalization (most intense bands in each spectrum have the same “height”). (b) SERS intensity of the 1228 cm⁻¹ band (highlighted in gray) of MBC in the Ag colloid as a function of MBC concentration and (c) in the logarithmic scale.

The average intensity of the last two concentrations is higher than the previous ones (Figure 1b). However, the standard deviation is also considerably higher, indicating significant uncertainty in the measurement. Additionally, after the measurements, both the microcentrifuge tube and the pipette tip contained precipitates from colloidal dispersion. This can happen because colloidal dispersions have a critical coagulation concentration (CCC), which is the threshold concentration at which precipitation occurs due to extensive aggregation [14]. In this case, the addition of large volumes of MBC no longer leads to an increase in the intensity of the SERS signal.

3.1.2. UV-Vis Extinction

In the UV-Vis extinction measurements in the absence of salt, the 400 nm band, which is assigned to isolated spherical nanoparticles (with no interference from MBC or salt addition), and the transverse electron oscillation mode in the aggregates [15], undergo a continuous decrease in intensity with increasing concentrations (Figure 2a). The first concentration where the SERS signal could be observed coincides with the one where the 400 nm band started to decrease, which is consistent with the need to induce the aggregation of AgNPs to observe the SERS signal of MBC, as discussed earlier, once the quantity of isolated AgNPs decreases. The intensity of this band continues to decrease linearly up to 3.0×10^{-6} mol/L (Figure 2b). However, from this concentration onwards, the rate of decrease of extinction slows down, forming a kind of plateau where the decrease can still be observed but at a slower rate. This suggests a saturation of the AgNP aggregation process induced by the addition of MBC to the colloidal dispersion.

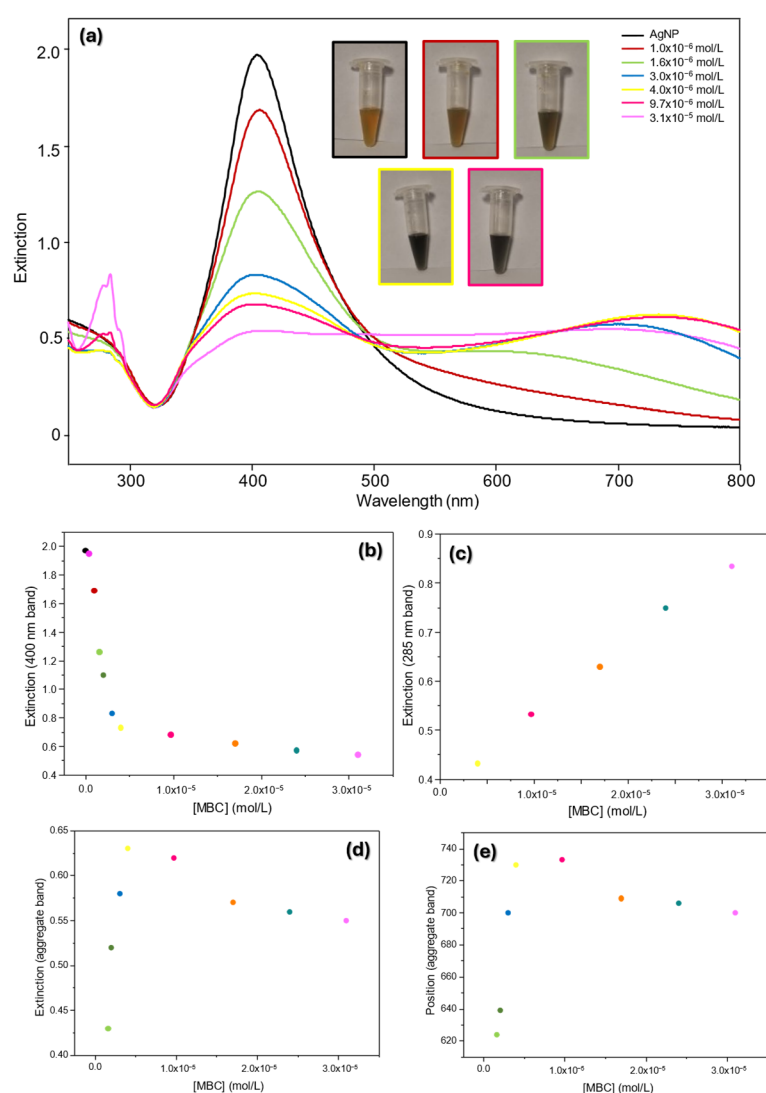


Figure 2. (a) Extinction spectra of the Ag colloid (diluted) in the presence of MBC (in the absence of salt). Inset: picture of the samples. (b) Intensity of the plasmon band at 400 nm as a function of the MBC concentration. (c) Intensity of the 285 nm band as a function of the MBC concentration. (d) Intensity of the maximum aggregate band as a function of the MBC concentration. (e) Position of the maximum aggregate band as a function of the MBC concentration.

At 1.0×10^{-6} mol/L, there is also a slight increase in extinction at longer wavelengths (>500 nm), which is related to aggregation caused by the addition of MBC. For the next concentration (1.6×10^{-6} mol/L), it is already possible to identify a band in this region, attributed to the longitudinal electron oscillation mode in the colloidal aggregates [15]. The extinction reaches a maximum at 4.0×10^{-6} mol/L, after which it begins to decrease, probably due to the excessive aggregation of colloidal dispersion. However, in the last two concentrations (2.4×10^{-5} and 3.1×10^{-5} mol/L, where the highest standard deviation was observed in the SERS measurements), the extinction remains more constant, aligning with the saturation of aggregation induced by the addition of MBC.

This band undergoes a shift with varying concentration at longer wavelengths, which becomes more evident from 1.6×10^{-6} mol/L (Figure 2e). The behavior is similar to intensity, as the band shifts toward longer wavelengths until 9.7×10^{-6} mol/L and starts decreasing from there, with a smaller variation in the last two concentrations (2.4×10^{-5} and 3.1×10^{-5} mol/L). This shift aligns with the formation of larger colloidal aggregates, and in [15], the authors associate such a shift with the growth of aggregates in a preferentially branched structure. However, no evident morphological differences were observed with TEM for the intensity decrease from 9.7×10^{-6} mol/L.

Another relevant point in the analysis is that the 285 nm band (π - π^* transition of the benzimidazole group) emerges from 4.0×10^{-6} mol/L onwards [16], attributed to the excess of MBC in colloidal dispersion (Figure 2c). It is also at this concentration that the SERS intensity reaches the saturation plateau, consistent with the hypothesis that excess MBC no longer effectively contributes to the SERS signal but rather to a conventional Raman signal. Thus, the intensity of the absorption band increases linearly with the MBC concentration.

3.1.3. TEM Images

The Ag colloid in the absence of MBC predominantly consists of isolated AgNPs or small aggregates (Figure 3a). The formation of these aggregates may be associated with the grid drying process or occur naturally, even though the UV-Vis extinction spectrum does not show signs of aggregation in this situation, as the formation of bands at longer wavelengths is not observed.

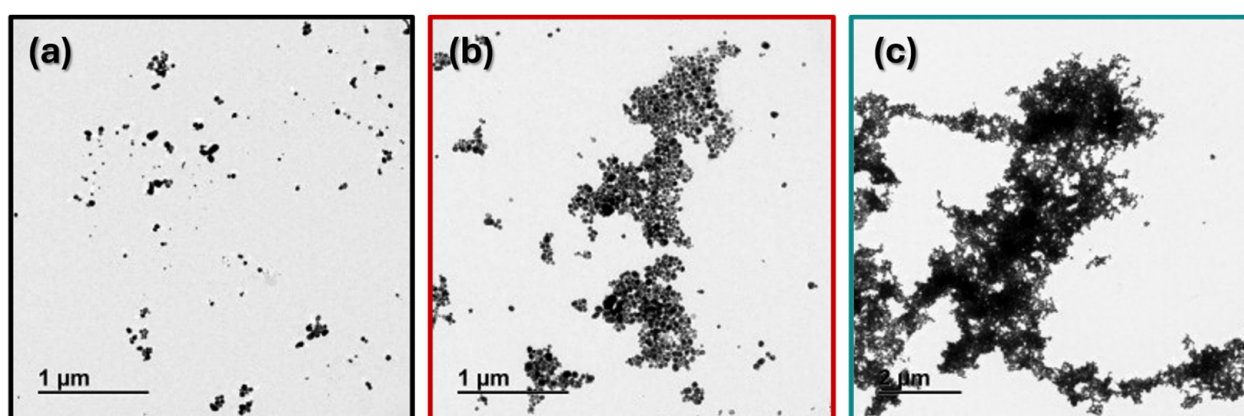


Figure 3. TEM microscopy images of the Ag colloid (not diluted) (a) in the absence of MBC and in the presence of MBC (b) 1.0×10^{-6} mol/L and (c) 2.4×10^{-5} mol/L. All are in the absence of salt.

At 1.0×10^{-6} mol/L, the first SERS signal is observed, although it is not very intense. In the TEM images, it is possible to observe the formation of aggregates (Figure 3b), but they do not have a high density of nanoparticles. Additionally, their morphology is closer to being compact (as opposed to a more branched morphology). In the UV-Vis extinction spectrum, the 400 nm band experiences an initial decrease in intensity, and a slight increase at longer wavelengths (>500 nm) can be identified, but the band is still indistinct, indicating low aggregation.

On the other hand, at 4.0×10^{-6} mol/L (Figure S2b), the aggregates are considerably larger than in the previous cases and have a more branched morphology, suggesting a transition from compact to branched morphology, preferably between 1.6 and 4.0×10^{-6} mol/L. In SERS, 4×10^{-6} mol/L is the concentration after the maximum intensity, but still exhibits high intensity, suggesting that preferably compact aggregates (with dimensions up to about $3 \mu\text{m}$) enable a more intense SERS signal for MBC. In the UV-Vis extinction spectrum, the aggregate band has the highest intensity, with its maximum at 730 nm.

At 9.7×10^{-6} mol/L (Figure S2c), more branched aggregates are predominantly observed, which grow with increasing MBC concentrations. Additionally, areas with higher particle density compared to lower concentrations are also evident. The intensity of the UV-Vis extinction band for these aggregates is similar to the previous concentration (4.0×10^{-6} mol/L) and exhibits the greatest shift among all samples, peaking at 733 nm. In SERS, this sample is already part of the plateau with little variation in intensity.

At 2.4×10^{-5} mol/L, there is a predominance of more branched aggregates, with regions showing higher particle density (Figure 3c). This concentration exhibited a significant standard deviation in SERS measurements. In the UV-Vis extinction spectra, the aggregate band reaches its maximum at 706 nm, with an intensity that falls within the plateau formed after the maximum intensity at 4.0×10^{-6} mol/L.

In their work, Lin et al. [17] studied the aggregation of nanoparticles in Au colloids charge-stabilized with citrate ions, SiO_2 charge-stabilized with OH^- and SiO^- , and polystyrene latex charge-stabilized with carboxylic acid groups by adding pyridine, NaCl, and HCl, respectively. Sánchez-Cortés et al. [18] used DMC-1,5-dimethylcytosine as an aggregating agent for additions to Ag colloids. In their discussions, both agree that at lower concentrations of the aggregating agent, the surface charge density on the nanoparticle surface is higher, causing electrostatic repulsion and leading to a few sites being available for adsorption. For this reason, not all collisions between nanoparticles will result in aggregation, and the mechanism governing aggregation is RLCA (reaction-limited cluster aggregation). On the other hand, at high concentrations of the aggregating agent, the surface charge density on the nanoparticles becomes lower, so the diffusion time is the limiting factor in the aggregation process, named DLCA (diffusion-limited cluster aggregation), and more collisions between clusters will result in aggregation. However, there is a difference in the type of aggregate resulting from each process based on their morphology. For DLCA (diffusion-limited cluster aggregation), Lin et al [17], observed that more branched aggregates are formed, while for RLCA, the aggregates are more compact. Sánchez-Cortés et al. [18], observed the opposite. For DLCA, more compacted aggregates are formed, while for RLCA, the aggregates are more branched. Moreover, Sánchez-Cortés et al. [18], associate the formation of the aggregate band at longer wavelengths in the UV-Vis extinction spectrum with the formation of more branched aggregates but at lower concentrations of the aggregating agent.

In the present work, more branched aggregates were observed in general at higher MBC concentrations. The presence of less superficial charges due to more adsorbed analyte molecules suggests a DLCA aggregation mechanism, leading us to the hypothesis that there is not a universal aggregate morphology based exclusively on an aggregation mechanism

(DLCA or RLCA), as the chemical nature of the aggregating agent must also be taken into consideration. At the same time, the aggregate band, which is related to the created branched aggregates, in the UV-Vis extinction spectra is localized at higher wavelengths for higher MBC concentrations. The same UV-Vis trend was observed by Sánchez-Cortés et al. [18], using DMC, although for lower DMC concentrations. The difference between the aggregation mechanisms observed previously and those presented here is attributed to the different effects that the adsorbed molecule could have on the specific aggregation of metal nanoparticles depending on the chemical structure of the adsorbate and the possibility of establishing intermolecular interactions on the interface.

3.1.4. DLS

The analysis of the size distribution of AgNPs and their aggregates as a function of MBC concentration in the absence of salt reveals a shift towards larger sizes at lower concentrations (Figure 4). At 1.3×10^{-6} mol/L (a concentration close to the one where the SERS signal was first observed— 1.0×10^{-6} mol/L), a more pronounced shift occurs, and from this concentration onwards, only small size oscillations were observed, remaining within the range between 153 ± 74 nm and 199 ± 83 nm. The difference observed in the aggregates' size in zeta potential and TEM images can be attributed to the equipment range of analysis (0.3 nm–5 μ m).

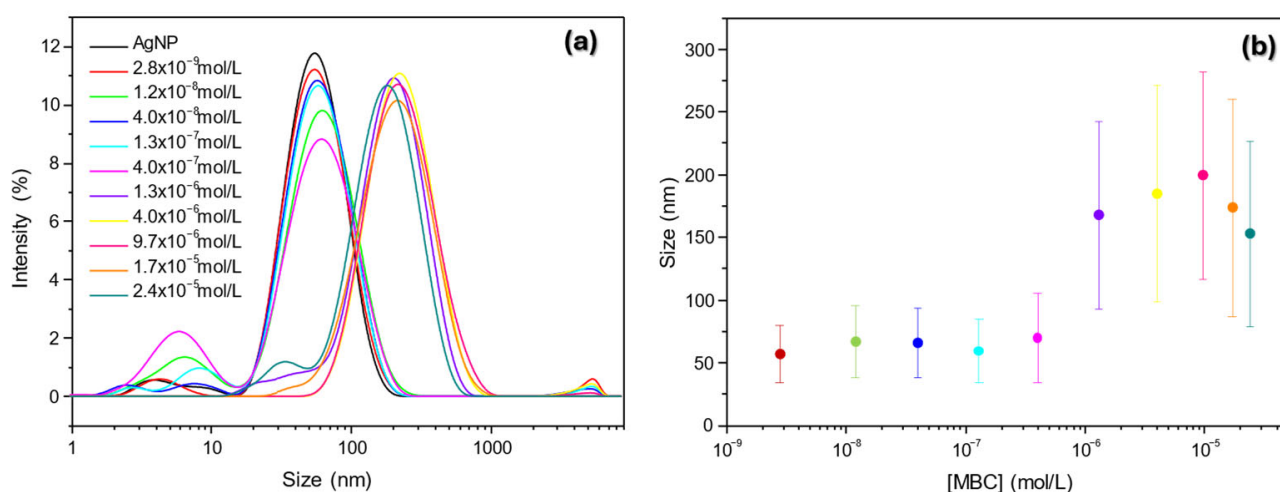


Figure 4. (a) Size distribution (histogram) of the AgNPs and their aggregates by percentage of intensity in a Ag colloid (diluted) in the presence of MBC and in the absence of salt and (b) the size of Ag colloid particles (AgNPs and their aggregates) as a function of MBC concentration.

3.1.5. Zeta Potential

The zeta potential of the Ag colloid as a function of the MBC concentration in the absence of salt becomes less negative (Figure 5). Since MBC has two pKa values (4.5 and 10.6), it predominantly exists as a neutral species at the pH levels in this study (pH \sim 5.5) [9]. Thus, with the increases in MBC concentration and aggregation, chloride ions, which surround the AgNPs (negative charge), may be replaced by MBC molecules, causing the surface charge to become less negative, as suggested by Lin et al. [17] and Sánchez-Cortés et al. [18]. Again, a more pronounced change can be identified for the last five samples, with concentrations ranging from 1.3×10^{-6} to 2.4×10^{-5} mol/L, resulting in AgNP aggregation, since a less negative zeta potential indicates reduced electrostatic repulsion between them.

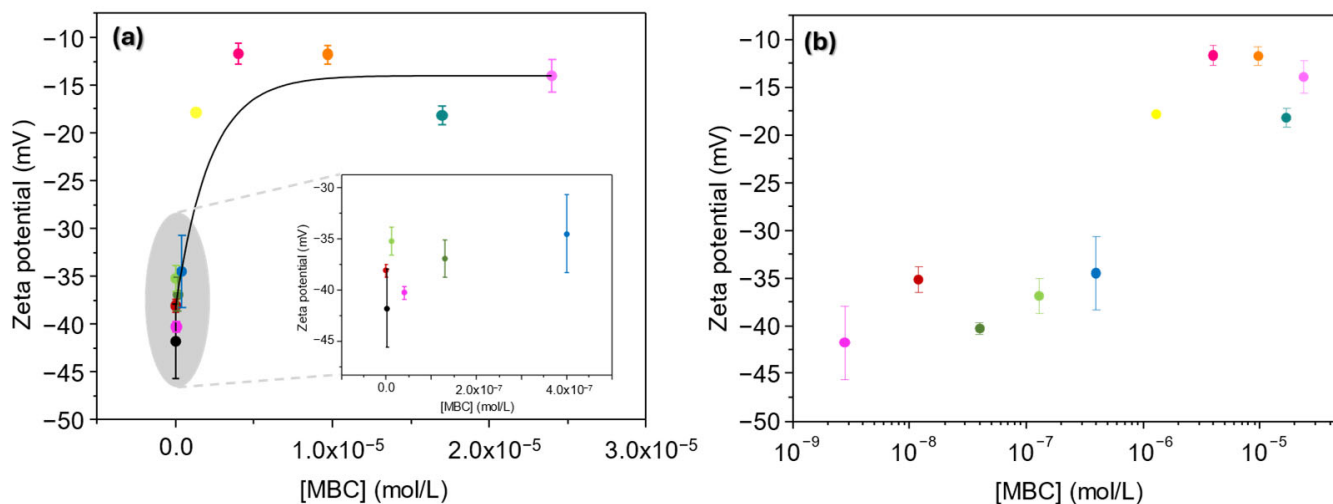


Figure 5. Zeta potential of the Ag colloid (in the absence of salt) (a) as a function of the MBC concentration (Inset: lower concentrations) and (b) in the logarithmic scale.

3.2. SERS in the Presence of Salt Without Ag Colloid Dilution

Aiming to detect MBC at lower concentrations, SERS measurements were performed in the presence of salt without the dilution of the Ag colloid, as described in the Experimental Section. In this case, the salt was added directly to the Ag colloid and, shortly thereafter, MBC was added. For this methodology, it was also possible to obtain the SERS signal starting from 4×10^{-6} mol/L (Figure S3). Therefore, this procedure did not allow the SERS signal to be obtained at lower concentrations. One possible explanation for this is that strong aggregation may have occurred because of the direct addition of salt to the Ag colloid. This intense aggregation could lead to the formation of aggregates bearing a non-suitable morphology to obtain an acceptable SERS signal. For this reason, the addition of salt in the Ag colloid diluted with the addition of water was also evaluated.

3.3. In the Presence of Salt: Dilution with Water Before Aggregation with KNO₃

3.3.1. SERS

The lowest concentration at which a SERS signal was seen was 1.3×10^{-6} mol/L (critical concentration for SERS). With the increase in MBC concentration, there is also an increase in the SERS intensity (measured by the band at 1228 cm^{-1} , which is related to the stretching of the O-CH₃ functional group [9]). This increase continues more significantly up to the concentration of 1.7×10^{-5} mol/L, when it then slows down (Figure 6b), tending to a stability plateau of the SERS signal intensity.

An adsorption isotherm is defined as the relationship between the concentrations of the analyte in the fluid phase and the adsorbent particles at equilibrium at a given temperature (Figure S4) [19]. Since SERS intensity is proportional to the number of analyte molecules adsorbed on the surface of the AgNPs, we can relate Figure 6b to an adsorption isotherm. The curve in Figure 6b tends to be described by the Langmuir-type isotherm (L2—Figure S4) [19]. As the MBC concentration increases, the surface of the AgNPs is gradually covered, increasing the SERS signal intensity. When complete coverage is reached, there are two possibilities: the formation of multilayers or excess unadsorbed analytes. In the first case, the analytes adsorbed in adjacent layers contribute little to the SERS signal due to their distance from the surface of the AgNPs, leading to the formation of a plateau. In the second case, the unadsorbed analytes contribute to the Raman signal, also leading to the formation of the plateau. The appearance of a 285 nm band in extinction spectra in UV-Vis (discussed in the next section) points to the second scenario in our analysis.

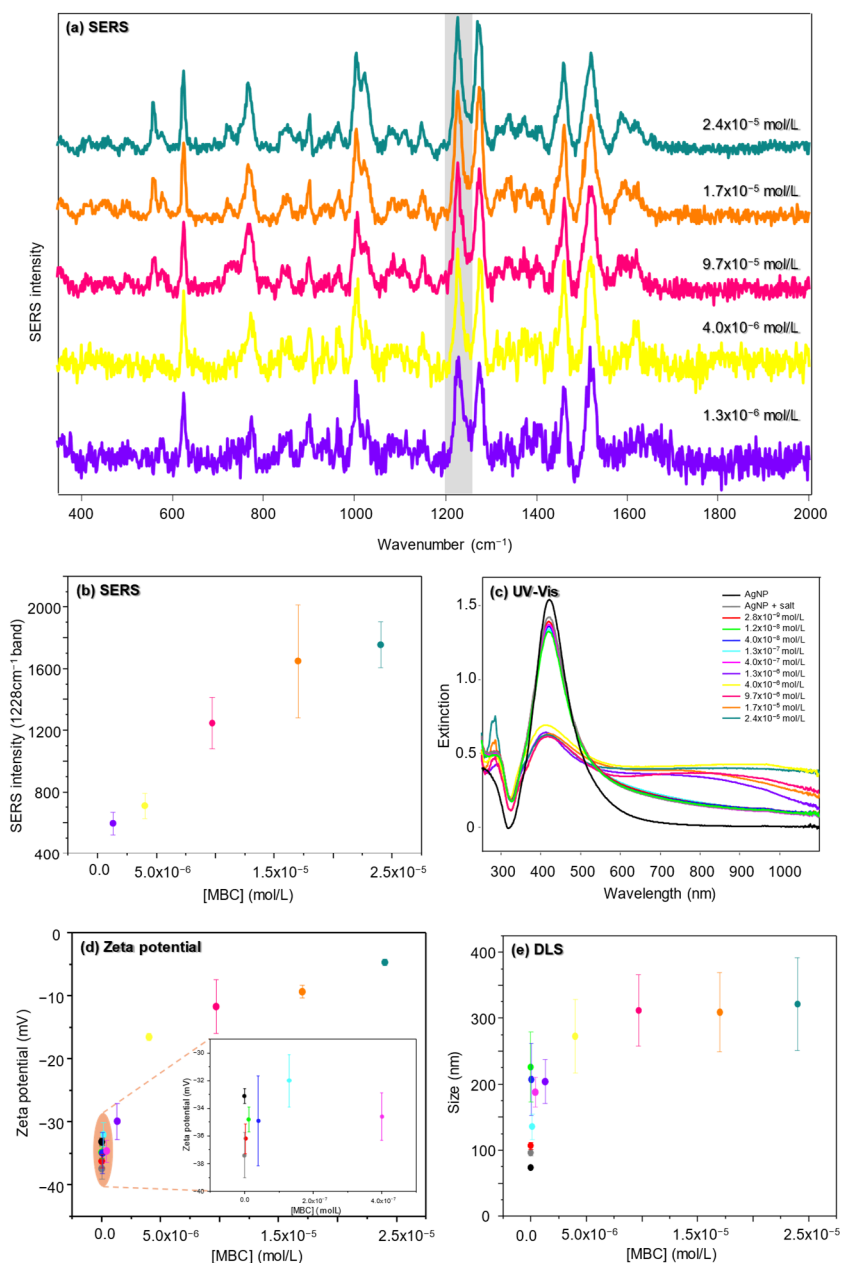


Figure 6. (a) SERS spectrum of MBC. Laser power: 10%, 10 s acquisition, $50\times$ lens, 785 nm laser, and 1 accumulation. Spectra with baseline correction and normalized (most intense bands in each spectrum have the same “height”). (b) SERS intensity (peak height) of the 1228 cm^{-1} band (highlighted in gray) as a function of MBC concentration in the Ag colloid. (c) Extinction spectra of Ag colloid particles (AgNPs and their aggregates) as a function of the MBC concentration. (d) Zeta potential of the Ag colloid as a function of the MBC concentration (inset: lower concentrations). (e) Size of the Ag colloid particles (AgNPs and their aggregates) as a function of the MBC concentration. All measurements are in the presence of salt (dilution with water before aggregation with salt).

3.3.2. UV-Vis Extinction

For UV-Vis extinction, the intensity of the $\sim 400\text{ nm}$ band decreases slightly with the addition of MBC compared to the isolated Ag colloid (Figure S5), remaining approximately constant up to $1.2 \times 10^{-8}\text{ mol/L}$. At $1.3 \times 10^{-6}\text{ mol/L}$, it undergoes a more significant decrease, reaching its stability plateau. For the band at longer wavelengths, its formation could be observed from the concentration of $1.3 \times 10^{-6}\text{ mol/L}$. Before this, extinction increased but without the formation of a band. At $1.3 \times 10^{-6}\text{ mol/L}$, we first observe the SERS signal of MBC under these conditions, corroborating the hypothesis of greater

aggregation from then on. Additionally, a band at 285 nm is formed, attributed to the excess MBC molecules in the colloidal dispersion. The appearance of this band occurs at 1.3×10^{-6} mol/L, the concentration at which the band at longer wavelengths starts to be seen, as well as the SERS signal of MBC. Figure S7 presents a comparison between the SERS intensity and the UV-Vis spectra of samples prepared in the absence and presence of salt, with dilution prior to aggregation for better comprehension.

3.3.3. Zeta Potential

The zeta potential study of the Ag colloid in the presence of salt as a function of the MBC concentration showed that the surface charges become less negative with increasing concentration. This change occurs from 1.3×10^{-6} mol/L (Figure 6d). Below this concentration, the zeta potential varies between -40 mV and -30 mV (Ag colloid without salt = -33.1 ± 0.5 mV; Ag colloid with salt = -37.4 ± 1.6 mV; MBC [2.8×10^{-9} mol/L] = -36.2 ± 1 mV; MBC [1.3×10^{-6} mol/L] = -29.9 ± 2.9 mV). The stability of the Ag colloid can be observed when the zeta potential values are higher than $+30$ mV or lower than -30 mV [20]. The change to less negative zeta potential values indicates that there may be coverage of the AgNPs' surface, where the surface charges are replaced by MBC molecules. This behavior is observed at the same concentrations where it was possible to obtain the SERS signal (MBC [4×10^{-6} mol/L] = -16.5 ± 0.6 mV; MBC [2.4×10^{-5} mol/L] = -4.6 ± 0.5 mV) and where the greatest changes in UV-Vis spectroscopy were observed, indicating changes in the aggregation of AgNPs. Indeed, the less negative values of the zeta potential with increasing MBC concentration are at the origin of the Ag colloid aggregation process. Figure S6a,b present a comparison of zeta potential measurements in linear and logarithmic scales for better comprehension.

3.3.4. DLS

The DLS analysis showed that the size of the aggregates increases with the increase in MBC concentration (Figure 6e) (Ag colloid without salt = 73.5 ± 0.9 nm; Ag colloid with salt = 96.2 ± 5.2 nm; MBC [2.8×10^{-9} mol/L] = 106.8 ± 5.4 nm; MBC [2.4×10^{-5} mol/L] = 321.4 ± 70 nm). The growth reaches stability in the concentration range between 4.0×10^{-6} mol/L and 2.4×10^{-5} mol/L. It is important to note that these concentrations are the same for which a more significant change in extinction at the wavelength near 400 nm is observed, consistent with the aggregation of AgNPs by the addition of MBC. Figure S6c,d present a comparison of size measurements in linear and logarithmic scales for better comprehension.

3.4. In the Presence of Salt: Aggregation with Salt Before Dilution with Water

Another alternative way to prepare samples in the presence of salt tested here was by aggregating the Ag colloid with the addition of salt and then diluting it with water. Only after the dilution was MBC added to the colloidal dispersion. It was not possible to detect MBC by following this order of addition. One hypothesis for this is that by aggregating before diluting, as the salt is added directly to the Ag colloid without prior dilution, the aggregation of AgNPs occurs very intensely, forming large aggregates, which hinders SERS signal acquisition. In contrast, since the Ag colloid is diluted before the addition of salt, the aggregation occurs less intensely, favoring the acquisition of the SERS signal, as the aggregates formed are not as large as in the last case. According to Oliveira et al. [10], the formation of larger and more branched aggregates led to the stabilization of the SERS signal at higher concentrations of the analyte thiabendazole (TBZ) without salt in their measurements. Thus, it can be inferred that the formation of very large (micrometric) aggregates does not favor the acquisition of the SERS signal.

3.4.1. UV-Vis Extinction

When nitrate is added to the Ag colloid before dilution in water, the intensity of the extinction band at ~ 400 nm significantly decreases with the addition of salt compared to the starting Ag colloid (Figure 7a,b). Additionally, a visual change in the colloid's color can be observed, turning dark quickly, followed by a loss of color and the formation of precipitates. With the addition of MBC, the intensity decreases a bit more, reaching its minimum at 1.2×10^{-8} mol/L of MBC, where it reaches a stability plateau, which can be related to the precipitation observed. For the band at longer wavelengths, however, there was a general increase in extinction at longer wavelengths with the addition of MBC. Both the slight decrease of the band at 400 nm and the overlap of the spectra at longer wavelengths (the region of aggregates or the transverse oscillation mode of electrons in the case of these AgNP aggregates) support the hypothesis of significant aggregation of the AgNPs caused by the addition of salt before the dilution of the colloid, as well as the insignificant contribution of the addition of MBC to this process.

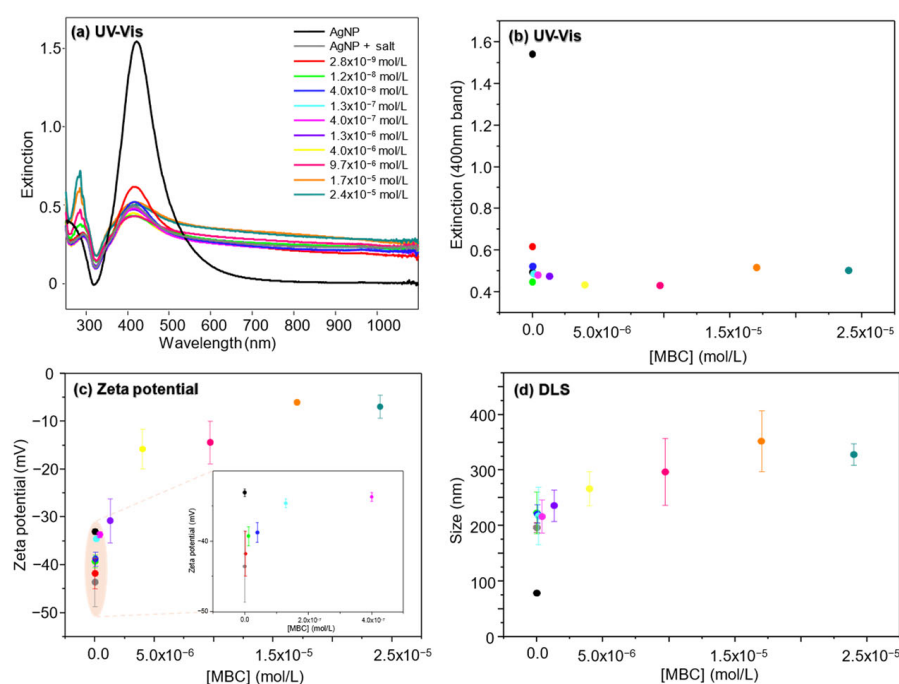


Figure 7. (a) Extinction spectra of Ag colloid particles (AgNPs and their aggregates) as a function of the MBC concentration and (b) intensity of the plasmon band at 400 nm as a function of the MBC concentration. (c) Zeta potential of the Ag colloid in the presence of MBC (inset: lower concentrations). (d) Size of Ag colloid particles (AgNPs and their aggregates) as a function of the MBC concentration. All measurements are in the presence of salt (aggregation with salt before dilution with water).

The appearance of the band at 285 nm occurs at 1.2×10^{-8} mol/L, the same concentration at which the extinction reaches its stability plateau. This indicates that at this concentration, there is an excess of MBC molecules in the colloidal dispersion, which do not contribute to the SERS signal (only to the Raman signal, which is much weaker). This occurs at the very lowest concentrations, indicating that even at higher concentrations, the aggregation of the AgNPs would not be favored, and consequently, neither would the SERS signal.

3.4.2. DLS

For this procedure, the addition of salt already promotes a considerable increase in the size of the populations (Figure 7d—Ag colloid without salt = 78.4 ± 1.4 nm; Ag colloid with salt = 196.3 ± 7.9 nm), consistent with the UV-Vis measurements. For the additions of

MBC, the growth occurs more gradually, reaching some stability at higher concentrations (MBC [2.8×10^{-9} mol/L] = 196.6 ± 9 nm; MBC [2.4×10^{-5} mol/L] = 328.4 ± 19.7 nm). This behavior supports the hypothesis of significant aggregation caused by the addition of salt to the Ag colloid before dilution.

3.4.3. Zeta Potential

The zeta potential study of the Ag colloid in the presence of salt as a function of MBC concentration showed that the surface charges become less negative with increasing concentrations. Similarly, the zeta potential varies between -40 mV and -30 mV up to 1.3×10^{-6} mol/L (Figures 7c and S8), with a subsequent decrease (in magnitude) for higher concentrations (Ag colloid without salt = -33.1 ± 0.5 mV; Ag colloid with salt = -43.6 ± 5.09 mV; MBC [2.8×10^{-9} mol/L] = -41.8 ± 3.18 mV; MBC [2.4×10^{-5} mol/L] = -7 ± 2.4 mV). The addition of salt does not induce a significant alteration (decrease in magnitude) of the zeta potential for the Ag colloid (average value).

4. Discussion

Absence of salt—the first SERS signal was obtained at 1.0×10^{-6} mol/L, with a linear increase in signal intensity as a function of the MBC concentration until 3.0×10^{-6} mol/L, where it reached its saturation plateau. The 400 nm band in UV-Vis extinction spectra decreases in intensity as a function of the MBC concentration until 3.0×10^{-6} mol/L, when a kind of plateau is formed. From 4.0×10^{-6} mol/L onwards, a band at 285 nm can be observed, which is related to the excess of MBC in the colloidal dispersion. The shift to higher wavelengths of the aggregate bands is related to the formation of more branched aggregates, as can be seen in TEM images, and occurs at higher concentrations. This means that less superficial charges are present in Ag nanoparticles (as observed in zeta potential measurements), suggesting that DLCA is the predominant aggregation mechanism.

Presence of salt without dilution—the SERS signal was first obtained at a concentration of 4×10^{-6} mol/L, showing that the direct addition of salt to a Ag colloid could favor the formation of large aggregates that are difficult to measure using SERS measurements.

Presence of salt: dilution before aggregation—the first SERS signal was obtained at 1.3×10^{-6} mol/L. For UV-Vis extinction, also at 1.3×10^{-6} mol/L, a more significant decrease in the 400 nm band can be observed, as well as the formation of bands at longer wavelengths and at 285 nm.

Presence of salt: aggregation before dilution—it was not possible to obtain a SERS signal. UV-Vis extinction measurements show that the intensity at the 400 nm band significantly decreases with the addition of salt compared to the original Ag colloid. At the same time, no band is formed at longer wavelengths. The appearance of the band at 285 nm occurs at 1.2×10^{-8} mol/L, indicating an excess of MBC even at the lowest concentrations.

5. Conclusions

In conclusion, the results showed that the addition of salt does not play a significant role in MBC SERS detection, as the best conditions were achieved in the absence of salt. In this scenario, more compact aggregates are associated with more intense SERS signals. In the presence of salt without Ag colloid dilution, the SERS signal did not improve compared to the absence of salt. However, when salt was present along with Ag colloid dilution, the order of dilution affected the SERS signal. No SERS signal was detected when salt was added to the Ag colloid before the addition of water. Conversely, when water was added to the Ag colloid before salt, a SERS signal was obtained, though at higher concentrations compared to in the absence of salt. Furthermore, it can be inferred that it

is not possible to establish a universal relationship between aggregate morphology and aggregation mechanisms; the analyte must be considered in the analysis.

Supplementary Materials: The following supporting information can be downloaded at: <https://www.mdpi.com/article/10.3390/chemosensors13010022/s1>, Table S1: Volume of the MBC stock solution added to the Ag colloid for the preparation of samples used in UV-Vis extinction, dynamic light scattering (DLS), and zeta potential measurements; Figure S1: Sample preparation: ESM method, in the absence of potassium nitrate and in the presence of potassium nitrate (with Ag colloid dilution); Figure S2: TEM microscopy images of the Ag colloid in the presence of MBC (a) 1.6×10^{-6} mol/L, (b) 4.0×10^{-6} mol/L, and (c) 9.7×10^{-6} mol/L. All are in the absence of salt; Figure S3: (a) SERS spectrum of MBC in a Ag colloid with the addition of salt and without dilution. Laser power: 10%, 10 s acquisition, 50 \times lens, 785 nm laser, and 1 accumulation. Spectra with baseline correction and normalized (most intense bands in each spectrum have the same “height”). SERS intensity (peak height) of the 1228 cm^{-1} band as a function of the concentration of MBC in a Ag colloid in (b) linear and (c) logarithmic scales; Figure S4: Classification scheme of isotherms taken from Giles et al. [19]; Figure S5: Intensity of the plasmon band at 400 nm as a function of MBC concentration in the presence of salt (diluting before aggregation) using (a) linear and (b) logarithmic scales; Figure S6: (a) Zeta potential of the Ag colloid as a function of the MBC concentration and (b) using the logarithmic scale. (c) Size of the Ag colloid particles (AgNPs and their aggregates) as a function of the MBC concentration and (d) using the logarithmic scale. All measurements are in the presence of salt (dilution with water before aggregation with salt); Figure S7: SERS intensity (a) in the absence of salt and (b) in the presence of salt (diluting before aggregation) and UV-Vis spectra (c) in the absence of salt and (d) in the presence of salt (diluting before aggregation); Figure S8: Zeta potential of the Ag colloid in the presence of MBC and in the presence of salt (aggregation with salt before dilution with water).

Author Contributions: Conceptualization, I.B.-C., M.J.d.S.O., C.S.M., S.S.-C., and C.J.L.C.; methodology, I.B.-C. and M.J.d.S.O.; software, I.B.-C. and M.J.d.S.O.; validation, I.B.-C. and M.J.d.S.O.; formal analysis, I.B.-C., M.J.d.S.O., C.S.M., S.S.-C., and C.J.L.C.; investigation, I.B.-C. and M.J.d.S.O.; resources, S.S.-C. and C.J.L.C.; data curation, I.B.-C. and M.J.d.S.O.; writing—original draft preparation, I.B.-C. and M.J.d.S.O.; writing—review and editing, I.B.-C., M.J.d.S.O., C.S.M., S.S.-C., and C.J.L.C.; visualization, I.B.-C. and M.J.d.S.O.; supervision, C.S.M., S.S.-C., and C.J.L.C.; project administration, S.S.-C. and C.J.L.C.; funding acquisition, S.S.-C. and C.J.L.C. All authors have read and agreed to the published version of the manuscript.

Funding: This research was funded by FAPESP (2018/22214-6, 2021/02746-6, and 2023/05423-9); CNPq (306501/2022-8); CAPES (88887.817533/2022-00); INCT/INEO. Ministerio de Ciencia, Innovacion y Universidades y FSE+ (PID2020-113900RB-I00 and PID2023146214OB-I00).

Institutional Review Board Statement: Not applicable.

Informed Consent Statement: Not applicable.

Data Availability Statement: Raw data are available upon request.

Acknowledgments: The authors gratefully acknowledge the support of the projects mentioned in the Funding Section above for this research.

Conflicts of Interest: The authors declare no conflicts of interest.

References

1. Anvisa (Agência Nacional de Vigilância Sanitária). Nota Técnica Conclusiva de Reavaliação do Carbendazim. Available online: https://www.gov.br/anvisa/pt-br/acessoainformacao/perguntasfrequentest/agrotoxicos/reavaliacao-de-agrotoxicos-2/copy_of_NotaTecnicaFinalcomseusanexos.pdf (accessed on 4 April 2023).
2. Ministério da Saúde. Carbendazim: Anvisa Concluiu Processo de Reavaliação e Mantém o Banimento. Available online: <https://www.gov.br/anvisa/pt-br/assuntos/noticias-anvisa/2022/carbendazim-anvisa-concluiu-processo-de-reavaliacao-e-mantem-o-banimento> (accessed on 4 April 2023).

3. Shi, J.; Li, C.; Jiang, Z. A new nanosurface molecularly imprinted polymer difunctional probe and on site generated gold nanosol SERS/RRS/Abs trimode determination of trace carbendazim. *Microchem. J.* **2024**, *196*, 109573. [[CrossRef](#)]
4. Wang, M.; Feng, J.; Ding, J.; Xiao, J.; Liu, D.; Lu, Y.; Liu, Y.; Gao, X. Color- and background-free Raman-encoded lateral flow immunoassay for simultaneous detection of carbendazim and imidacloprid in a single test line. *Chem. Eng. J.* **2024**, *487*, 150666. [[CrossRef](#)]
5. Luong, H.N.; Nguyen, N.M.; Tran, C.K.; Nguyen, T.T.; Nguyen, N.P.; Huynh, T.M.H.; Tran, T.T.; Phan, B.T.; Thi, T.V.T.; Dang, V.Q. Detection of carbendazim by utilizing multi-shaped Ag NPs decorated ZnO NRs on patterned stretchable substrate through surface-enhanced Raman scattering effect. *Sens. Actuators A Phys.* **2022**, *346*, 113816. [[CrossRef](#)]
6. Ma, C.-H.; Zhang, J.; Hong, Y.-C.; Wang, Y.-R.; Chen, X. Determination of carbendazim in tea using surface enhanced Raman spectroscopy. *Chin. Chem. Lett.* **2015**, *26*, 1455–1459. [[CrossRef](#)]
7. Chen, X.; Lin, M.; Sun, L.; Xu, T.; Lai, K.; Huang, M.; Lin, H. Detection and quantification of carbendazim in Oolong tea by surface-enhanced Raman spectroscopy and gold nanoparticle substrates. *Food Chem.* **2019**, *293*, 271–277. [[CrossRef](#)]
8. Furini, L.N.; Sanchez-Cortes, S.; López-Tocón, I.; Otero, J.C.; Aroca, R.F.; Constantino, C.J.L. Detection and quantitative analysis of carbendazim herbicide on Ag nanoparticles via surface-enhanced Raman scattering. *J. Raman Spectrosc.* **2015**, *46*, 1095–1101. [[CrossRef](#)]
9. Furini, L.N.; Constantino, C.J.L.; Sanchez-Cortes, S.; Otero, J.C.; López-Tocón, I. Adsorption of carbendazim pesticide on plasmonic nanoparticles studied by surface-enhanced Raman scattering. *J. Colloid. Interface Sci.* **2016**, *465*, 183–189. [[CrossRef](#)] [[PubMed](#)]
10. S Oliveira, M.J.; Bianchi-Carvalho, I.; GRubira, R.J.; Sánchez-Cortés, S.; LConstantino, C.J. Plasmonic Ag Nanoparticles: Correlating Nanofabrication and Aggregation for SERS Detection of Thiabendazole Pesticide. *ACS Omega* **2024**, *9*, 42571–42581. [[CrossRef](#)] [[PubMed](#)]
11. Leopold, N.; Lendl, B. A New Method for Fast Preparation of Highly Surface-Enhanced Raman Scattering (SERS) Active Silver Colloids at Room Temperature by Reduction of Silver Nitrate with Hydroxylamine Hydrochloride. *J. Phys. Chem. B* **2003**, *107*, 5723–5727. [[CrossRef](#)]
12. McCreery, R.L. *Raman Spectroscopy for Chemical Analysis*; Wiley: Hoboken, NJ, USA, 2000. [[CrossRef](#)]
13. Sánchez-Cortés, S.; García-Ramos, J.V.; Morcillo, G. Morphological Study of Metal Colloids Employed as Substrate in the SERS Spectroscopy. *J. Colloid Interface Sci.* **1994**, *167*, 428–436. [[CrossRef](#)]
14. Hsu, J.-P.; Liu, B.-T. Critical Coagulation Concentration of a Colloidal Suspension at High Particle Concentrations. *J. Phys. Chem. B* **1998**, *102*, 334–337. [[CrossRef](#)]
15. Blatchford, C.G.; Campbell, J.R.; Creighton, J.A. Plasma resonance—Enhanced raman scattering by absorbates on gold colloids: The effects of aggregation. *Surf. Sci.* **1982**, *120*, 435–455. [[CrossRef](#)]
16. Bodian, E.; Sarr, I.; Sambou, S.; Mendy, A.; Gueye, C.; Diop, C.; Diagne, I.; Thiaré, D.; Diaw, P.; Gaye-Seye, M.; et al. Spectrophotometric Method for the Determination of Carbendazim in Orange Juice Samples Marketed in Senegal. *Chem. Sci. Int. J.* **2017**, *21*, 1. [[CrossRef](#)]
17. Weitz, D.A.; Lin, M.Y.; Lindsay, H.M. Universality laws in coagulation. *Chemom. Intell. Lab. Syst.* **1991**, *10*, 133–140. [[CrossRef](#)]
18. Aroca Muñoz, R.F.; Campos Vallete, M.; García Ramos, J.V. *Amplificación Plasmónica de Espectros Raman y de Fluorescencia: SERS y SEF Sobre Nanoestructuras Metálicas*; Consejo Superior de Investigaciones Científicas: Madrid, Spain, 2014.
19. Giles, C.H.; MacEwan, T.H.; Nakhwa, S.N.; Smith, D. 786. Studies in adsorption. Part XI. A system of classification of solution adsorption isotherms, and its use in diagnosis of adsorption mechanisms and in measurement of specific surface areas of solids. *J. Chem. Soc. (Resumed)* **1960**, *846*, 3973–3993. [[CrossRef](#)]
20. Cunningham, D.; Littleford, R.E.; Smith, W.E.; Lundahl, P.J.; Khan, I.; McComb, D.W.; Graham, D.; Laforest, N. Practical control of SERRS enhancement. *Faraday Discuss.* **2006**, *132*, 135–145. [[CrossRef](#)] [[PubMed](#)]

Disclaimer/Publisher’s Note: The statements, opinions and data contained in all publications are solely those of the individual author(s) and contributor(s) and not of MDPI and/or the editor(s). MDPI and/or the editor(s) disclaim responsibility for any injury to people or property resulting from any ideas, methods, instructions or products referred to in the content.